

Article

Composite of α -FeOOH and Mesoporous Carbon Derived from Indian Blackberry Seeds as Low-Cost and Recyclable Photocatalyst for Degradation of Ciprofloxacin

Dimple P. Dutta ^{1,*}  and Sebin Abraham ²¹ Chemistry Division, Bhabha Atomic Research Centre (BARC), Trombay, Mumbai 400085, Maharashtra, India² Department of Chemistry, Indian Institute of Science Education and Research Bhopal, Bhopal Bypass Road, Bhauri, Bhopal 462066, Madhya Pradesh, India

* Correspondence: dimpled@barc.gov.in

Abstract: This study aims to analyse the use of biowaste-derived carbon in enhancing the photocatalytic effect of Earth-abundant visible light active goethite (α -FeOOH). The biowaste material used in this case is seeds of the Indian blackberry fruit. The FeOOH/C composite has been synthesized using an assisted sonochemical technique. The photocatalysts have been characterized using powder x-ray diffraction, nitrogen adsorption isotherms and scanning electron microscopy technique. FTIR and Raman studies have been carried out to understand the structure bonding correlation. The band gap has been ascertained using Tauc plots. The adsorption and consequent photodegradation of CIP have been studied via UV-visible spectroscopy and the mechanism has been ascertained by using radical quenching techniques. The charge separation efficiency has been ascertained through photoluminescence (PL) studies and electrochemical impedance studies (EIS). The pivotal role played by photogenerated holes (h^+) in the photocatalytic degradation of CIP has been highlighted. The low cost biowaste-derived carbon as a constituent of the FeOOH/C composite shows great promise as a supporting material for enhancing the photocatalytic properties of such semiconductor materials.

Keywords: photocatalyst; FeOOH; bio-derived carbon; composite



Citation: Dutta, D.P.; Abraham, S. Composite of α -FeOOH and Mesoporous Carbon Derived from Indian Blackberry Seeds as Low-Cost and Recyclable Photocatalyst for Degradation of Ciprofloxacin. *Catalysts* **2023**, *13*, 191. <https://doi.org/10.3390/catal13010191>

Received: 11 December 2022

Revised: 5 January 2023

Accepted: 11 January 2023

Published: 13 January 2023



Copyright: © 2023 by the authors. Licensee MDPI, Basel, Switzerland. This article is an open access article distributed under the terms and conditions of the Creative Commons Attribution (CC BY) license (<https://creativecommons.org/licenses/by/4.0/>).

1. Introduction

Pollution of water bodies is reaching mammoth proportions with increased urbanization and industrialization. Effluents from the textile, paint, leather, electroplating, pharmaceutical, battery manufacturing and various other industries contaminate water through the release of heavy metals, organic pollutants and antibiotics and pose a grave threat to the ecosystem. Particularly, with advances in medicine, the use of antibiotics to combat a plethora of bacterial disease has increased manifold. Antibiotics are widely used in medical care for both humans and animals and are also found used extensively in farming. A considerable portion of the ingested antibiotics is excreted from the human/animal body and enters wastewater. Poor recycling strategies for expired antibiotics also adds to environmental pollution. Bacteria develops resistance towards antibiotics through genetic mutation, which acts as a protective mechanism for its survival and propagation, which poses a grave threat to the ecosystem [1]. Hence, it is imperative that antibiotics and their metabolites are completely removed from wastewater to protect the environment.

Among the various classes of antibiotics, quinolones are considered to be a broad-spectrum antibiotic finding application for combating bacterial infections in the urinary bladder, lungs, intestines and skin, as well as the digestive and skeletal systems. Ciprofloxacin (CIP) is a fluoroquinolone-based antibiotic that has an optimum oral intake and is commonly used for bacterial infection in both humans and animals [2]. However, when ingested, CIP is only partially degraded to its metabolites and, in nature, it mostly remains

in its original form. It is present in wastewater and is not effectively removed in wastewater treatment plants. Hence, efforts are needed to combat this problem, as its long-term presence in water bodies may lead to the development of resistance in bacteria to this class of antibiotics. Methods like coagulation or filtration are not suitable for the removal of antibiotics from wastewater [3]. However, visible light photocatalysis using semiconductor types of material is an effective way to decontaminate water and has been used for the degradation of a variety of organic pollutants [4–7]. It should be noted that photocatalysts that are active in visible light are generally obtained by suitable cation/anion doping of metal oxides like TiO_2 , ZnO , etc., or via formation of heterojunction composites [8]. CIP photodegradation has been reported using CeO_2/ZnO and $\text{CeO}_2\text{-Ag/AgBr}$ nanocomposites [9,10]. The problem lies in the fact that the synthesis of these artificially doped and nanocomposite systems leads to higher cost. Hence, for practical applications, less expensive and non-toxic photocatalysts like goethite ($\alpha\text{-FeOOH}$), which is commonly available in Earth's crust, can be a good substitute [11]. The band gap of natural goethite is ~ 2.1 eV and it forms photogenerated charge carriers with visible light irradiation [12]. However, the photocatalytic proficiency of $\alpha\text{-FeOOH}$ is low due to the inherent aggregation of particles and its inability to efficiently separate the photogenerated charge carriers. Efforts to disperse it in a conducting matrix have been attempted and there are reports on degradation of CIP using graphene quantum dots (GQDs)-doped goethite ($\alpha\text{-FeOOH}$) nanocomposites via a H_2O_2 -assisted photo Fenton process [13]. In this work, the conducting matrix for $\alpha\text{-FeOOH}$ is mesoporous carbon obtained from seeds of Indian blackberry (*Syzygium cumini*) fruit [14]. The Indian blackberry plants are found abundantly in southeast Asia and the black color edible fruit contains seeds that are normally discarded. These seeds have been found to be a good precursor source of carbon, which can be used for fluoride ion removal from water [15]. The inexpensive carbon source and facile synthesis makes the process advantageous for practical application. CIP photodegradation has been attempted using this FeOOH/C composite and the results obtained have been compared with that of $\alpha\text{-FeOOH}$. The details of the mechanism of the photodegradation process have been proposed based on the experimental results obtained.

2. Results and Discussion

2.1. X-ray Diffraction, Raman, FTIR and Surface Area Analysis

The powder XRD patterns of carbon derived from Indian blackberry seeds, FeOOH and the FeOOH/C composite are shown in Figure 1a. The diffraction peaks correspond to orthorhombic Goethite $\alpha\text{-FeOOH}$ (ICSD # 239321) with space group P_{bnm} . The lattice parameters are found to be $a = 4.595$ Å, $b = 9.942$ Å and $c = 3.01$ Å. The biomass-derived carbon exhibits a large, broad peak at $\sim 23^\circ$, which arises due to diffraction from the (002) plane, and a very low intensity peak at $\sim 43^\circ$ due to the graphitic (001) plane. The amorphous nature of the carbon is very prominent, and it has few graphitic domains. The FeOOH/C composite shows signature peaks of goethite $\alpha\text{-FeOOH}$ and the broad amorphous carbon peak at $\sim 23^\circ$ is visible in the background. No other peaks pertaining to any impurity are visible in the samples. The presence of carbon in the FeOOH/C composite is confirmed via Raman spectroscopy. The Raman spectra of carbon and the FeOOH/C composite are shown in Figure 1b. For the biomass-derived carbon, the Raman spectrum exhibits a D-band at ~ 1347 cm^{-1} and a G-band at ~ 1578 cm^{-1} . The former arises due to the A_{1g} vibration of carbon aromatic rings and signifies the disorder/defects present in the carbon. The latter is a signature of the E_{2g} mode of vibration of the sp^2 C-C bond and represents the existence of an ordered graphitized structure [16]. The ratio of the corresponding intensity I_D/I_G of the bands is 1.01 and is indicative of the presence of additional defects in the carbon sample. In the FeOOH/C composite, apart from the carbon D- and G-bands at ~ 1346 and ~ 1582 cm^{-1} , respectively, a relatively strong peak at ~ 387 cm^{-1} , along with other low intensity peaks at 241, 299, 471, 549 and 689 cm^{-1} , are visible. The latter are all signature Raman peaks of Goethite $\alpha\text{-FeOOH}$ arising due to A_g and B_{2g} symmetry [17]. The I_D/I_G ratio in the composite increases to 1.07, which signifies increased disorder in the carbon component.

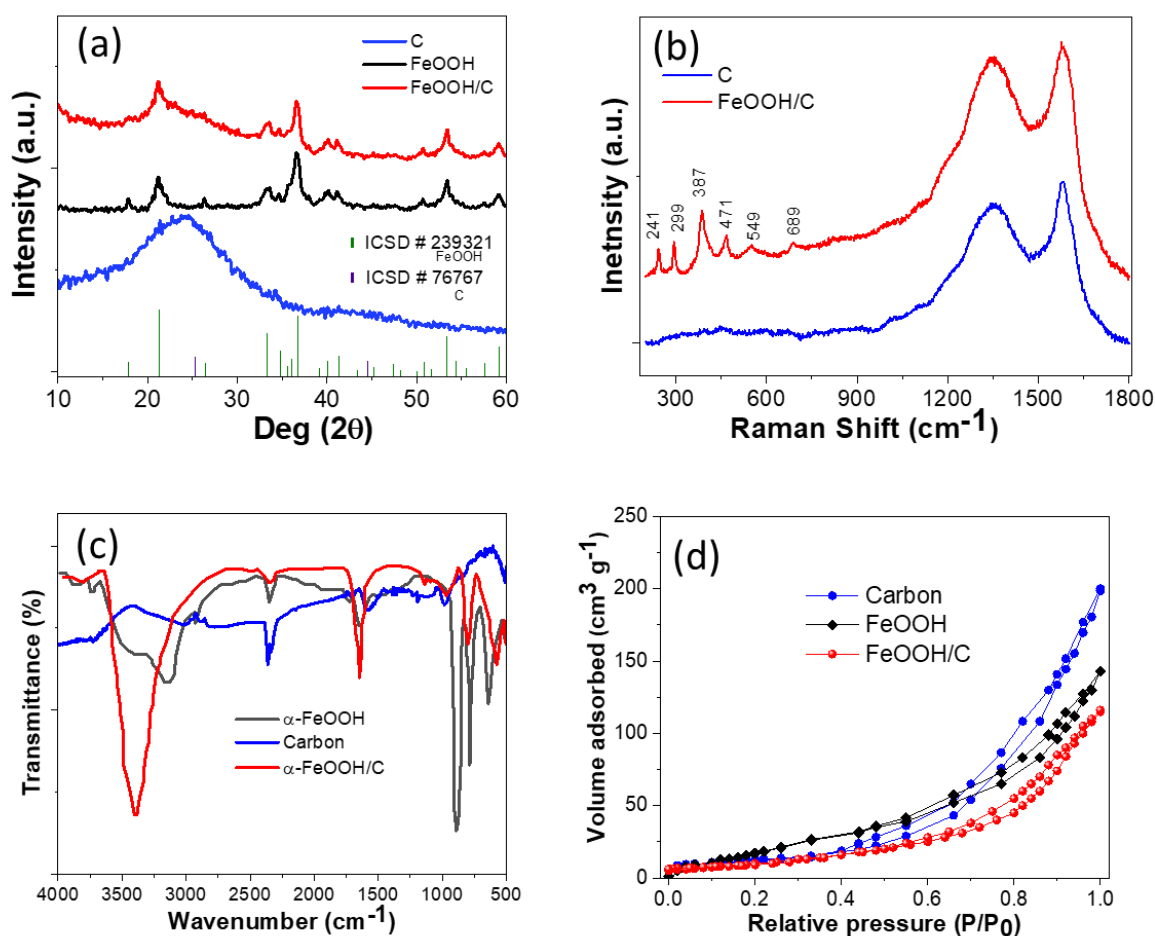


Figure 1. (a) Powder XRD of carbon, α -FeOOH and the FeOOH/C composite, (b) Raman spectra of carbon and the FeOOH/C composite, (c) FTIR spectra and (d) BET adsorption isotherm of carbon, α -FeOOH and the FeOOH/C composite.

FTIR spectra of carbon derived from Indian blackberry seeds, α -FeOOH and the FeOOH/C composite are shown in Figure 1c. The broad peak between 3000–3500 cm $^{-1}$ in the case of α -FeOOH and the FeOOH/C composite pertains to O-H stretching from the compounds and also that from adsorbed moisture. α -FeOOH also shows prominent bands between 620–680 cm $^{-1}$ pertaining to ν_{symm} Fe-O and between 750–1000 cm $^{-1}$, which are due to ν_{bending} Fe-O-H [18]. The FTIR spectrum of carbon showed the presence of functional groups, which is a common occurrence if it is derived from biomass precursors. The broad band between 3400–2800 cm $^{-1}$ is due to the various stretching vibrations of C-H. The sharp peaks at 2341 and 2361 cm $^{-1}$ are O=C=O stretching vibrations arising probably due to surface-adsorbed CO $_2$. The broad peak ranging from 1650–1500 cm $^{-1}$ is due to C=O and C=C stretching vibrations [19]. The small peak at 976 cm $^{-1}$ is attributed to C=C bending. In the case of the FeOOH/C composite, the ν_{symm} Fe-O and ν_{bending} Fe-O-H peaks are slightly shifted, indicating that the addition of carbon leads to a change in the Fe-O and Fe-O-H bonds in α -FeOOH.

The surface area of carbon, α -FeOOH and the FeOOH/C composite was ascertained from the nitrogen adsorption isotherm via BET method and the corresponding values are given in Table 1. Type II isotherm with H3 hysteresis loop is obtained, indicating the presence of slit-shaped pores (Figure 1d). The mean pore diameter and total pore volume has been obtained via BJH analysis and the values are given in Table 1. The specific surface area of the FeOOH/C composite is higher than that of α -FeOOH, which is due to its dispersion on the carbon surface. This is beneficial since it leads to a greater number of photocatalytically active sites in the composites. The total pore volume of FeOOH/C

reduces compared to that obtained for the Indian blackberry seed-derived carbon and can be attributed to the blockage in some pores of the latter by incorporation of α -FeOOH.

Table 1. BET specific surface areas, mean pore diameters and total pore volumes of α -FeOOH, C and the α -FeOOH/C composite.

Samples	Specific Surface Area ($\text{m}^2 \text{g}^{-1}$)	Mean Pore Diameter (nm)	Total Pore Volume ($\text{cm}^3 \text{g}^{-1}$)
C	64.35	8.06	0.14
α -FeOOH	38.75	3.02	0.08
α -FeOOH/C	52.25	6.17	0.12

X-ray photoelectron spectroscopy (XPS) of the FeOOH/C composite sample was recorded to analyse the valence state of Fe. The survey spectrum in Figure 2a shows the presence of Fe2p, C1s and O1s binding energy peaks. The high resolution Fe2p XPS shows the presence of relatively higher intensity peaks at 712.4 eV and 726.2 eV corresponding to Fe 2p_{3/2} and Fe 2p_{1/2} binding energy peaks of Fe³⁺ [20]. The satellite peak of Fe 2p_{3/2} is distinctly visible at 718.6 eV.

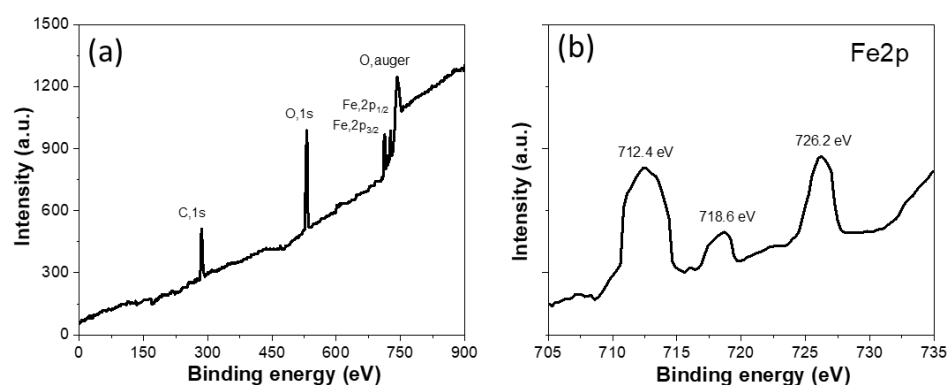


Figure 2. (a) XPS survey spectrum of the FeOOH/C composite, (b) high resolution Fe2p XPS of the FeOOH/C composite.

2.2. Morphological Study

The morphology of the samples was ascertained via SEM. The carbon exhibits a sheet-like structure with pores (Figure 3a,b). The pristine α -FeOOH is formed in the shape of nanorods with lengths between 100–150 nm (Figure 3c,d). In the case of the FeOOH/C composite, α -FeOOH nanorods can be seen scattered on the carbon surface, but their length is reduced to ≤ 100 nm (Figure 3e,f). This indicates that the size of α -FeOOH is affected by carbon addition, which acts as nucleation sites for the growth of the former and restricts the long nanorods formation. The contact between carbon and α -FeOOH is advantageous for the transfer and separation of charge carriers, which might enhance the photocatalytic process. Similar observations have been made in the case of β -FeOOH composites with carbon nanotubes [21]. The EDS of carbon, α -FeOOH and the FeOOH/C composite is shown in Figure 3g–i, respectively, which confirms the presence of only the constituent elements for each sample.

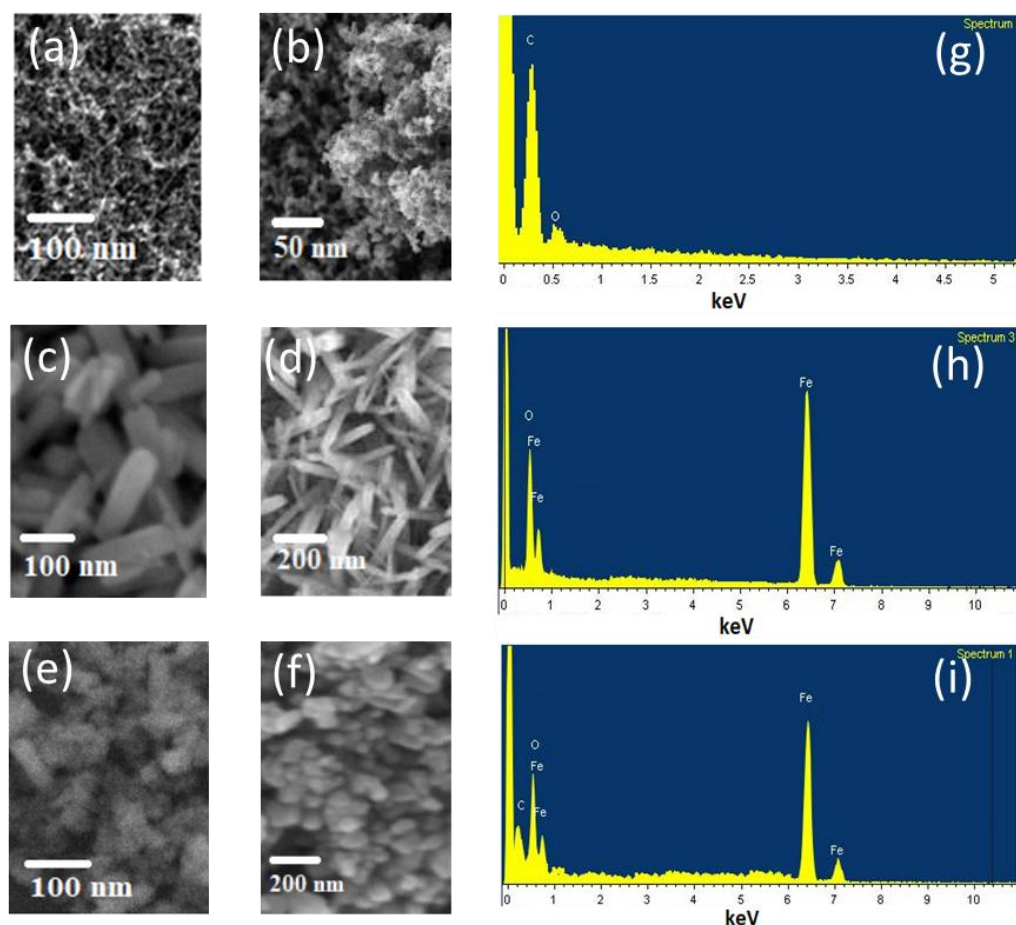


Figure 3. SEM of (a,b) carbon, (c,d) α -FeOOH and (e,f) the FeOOH/C composite, and EDS of (g) carbon, (h) α -FeOOH and (i) the FeOOH/C composite.

2.3. UV-Vis Absorption Analysis

The UV-visible absorption spectra of α -FeOOH and FeOOH/C is shown in Figure 4a. Both samples exhibit a strong absorption of visible light between 400–600 nm. The absorption in the visible portion is stronger in the case of the FeOOH/C composite. The band gap was obtained from the $(\alpha h\nu)^2$ vs. $h\nu$ plot and was found to be ~ 2.13 eV for α -FeOOH and ~ 2.08 eV for FeOOH/C. This indicates that the addition of carbon influences the optical property of α -FeOOH, which was previously reported in the case of β -FeOOH nanocomposites with carbon nanotubes (CNT) [21]. This can be ascribed to the alteration in Fe–O–H bonds in the FeOOH/C composites by the addition of carbon, which has also been corroborated by the FTIR studies. The greater extent of visible light absorption renders potentially better photocatalytic ability to the FeOOH/C composite.

The position of the conduction band (CB) and valence band (VB) was obtained from the following empirical equations [22,23]:

$$E_{VB} = \chi + E_e + 0.5E_g \quad (1)$$

$$E_{CB} = E_{VB} - E_g \quad (2)$$

where χ denotes the absolute electronegativity of the photocatalyst, E_e is 4.5 eV (energy of free electron) and E_g is the band gap. In the case of the FeOOH/C composite, E_{VB} and E_{CB} are calculated to be 2.92 eV and 0.84 eV, respectively.

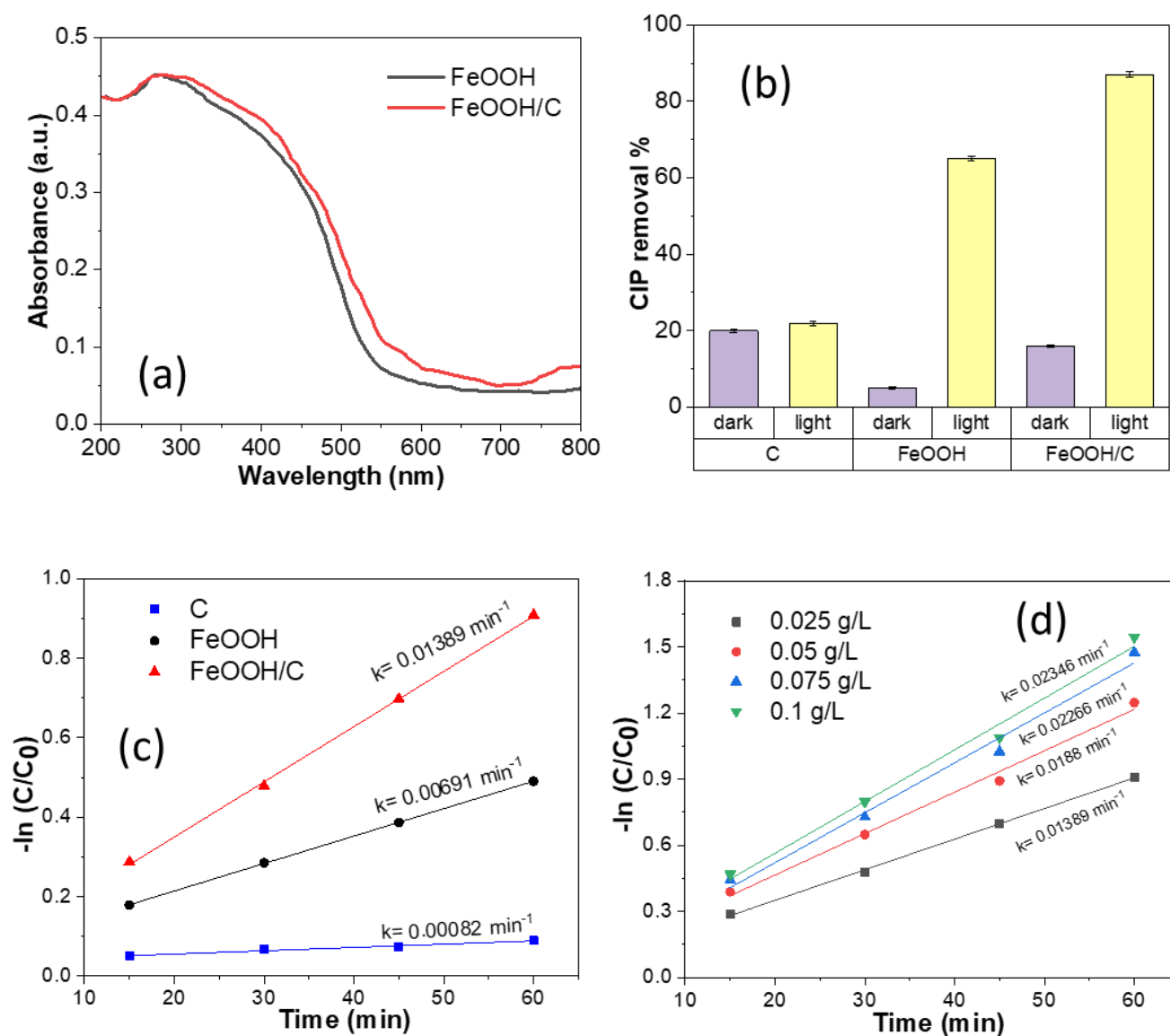


Figure 4. (a) UV-vis absorption spectra of carbon derived from Indian blackberry seeds, α -FeOOH and the FeOOH/C composite, (b) the extent of ciprofloxacin (CIP) by carbon, α -FeOOH and the FeOOH/C composite, (c) the plot of $-\ln([C]/[C_0])$ vs. t and (d) the effect of concentration of the FeOOH/C composite on the photodegradation of CIP.

2.4. Catalyst Activity

The extent of ciprofloxacin (CIP) removal by carbon derived from Indian blackberry seeds, α -FeOOH and the FeOOH/C composite in dark and under visible light within a total time period of 75 min (15 min in the dark followed by 60 min under visible light irradiation) is shown in Figure 4b. CIP removal by the sample in the dark pertains to its adsorption on the sample surface and it is highest in the case of carbon. This is readily explained based on its surface area, which is the largest among all the three materials tested, as is evident from the BET analysis. This facilitates the adsorption of a larger amount of CIP on the carbon surface. Under visible light irradiation, the CIP photodegradation was highest for the FeOOH/C composite. There was almost no photodegradation observed in the case of carbon. The minor 2% improvement in CIP removal is probably due to further adsorption of CIP on the carbon.

The kinetics of CIP photodegradation were calculated considering a pseudo-first order reaction model as given below:

$$\ln \frac{[C]}{[C_0]} = -kt \quad (3)$$

where C_0 and C represent the initial and final concentrations of CIP in the reaction mixture, t is the time elapsed since switching on the visible irradiation and k is the reaction rate constant. The k value is obtained from the slope of the plot of $-\ln([C]/[C_0])$ vs. t and is shown in Figure 4c. As per the results obtained, it is evident that the photodegradation rate constant for CIP in the case of the FeOOH/C composite is almost double than that of α -FeOOH.

The concentration of the FeOOH/C composite was varied (25, 50, 75 and 100 mg L⁻¹) and its effect on the photodegradation of CIP was monitored. As is evident from Figure 4d, there is a considerable increase in the efficiency of CIP removal when the concentration of the composite is increased from 25 mg L⁻¹ to 50 mg L⁻¹. However, the improvement in the rate of CIP removal is much less when the concentration of FeOOH/C is increased further to 75 and 100 mg L⁻¹. This is probably due to the enhancement in the scattering of the light by the photocatalyst particles when the concentration is increased. The optimum concentration of the FeOOH/C composite for CIP photodegradation is ~50–75 mg L⁻¹.

For better insight into the CIP degradation process by the FeOOH/C composite, the role of the reactive oxygen species viz. OH• (hydroxyl radicals) and h⁺ (holes with positive charge) has been evaluated. Tert-butanol (TBA) was used as a OH• scavenger and ammonium oxalate (AO) as an h⁺ scavenger [24]. The resulting kinetics plot is shown in Figure 5a. A decrease in the rate of CIP photodegradation is observed with the addition of TBA and AO, but the extent of the decrease is comparatively more in case of the latter. This indicates that, though OH• and h⁺ are both involved in the photocatalysis process, the latter plays a key role and acts as the primary oxidative species in the photodegradation of CIP. Since h⁺ is mostly present on the surface of the photocatalyst, it indicates that the photodegradation primarily takes place on CIP adsorbed on the FeOOH/C composite.

The photodegradation of CIP occurs through a series of stages. Initially, in the dark, there is adsorption of CIP on the surface of the photocatalyst. On irradiation with visible light, there is generation of a photoexcited electron (e⁻) and a photogenerated hole (h⁺) in the CB and VB of the photocatalyst, respectively. Efficient charge separation leads to the formation of O₂^{-•} (superoxide radical anion) and HO₂[•] (hydroperoxyl radical) by the reaction of e⁻ with O₂. These further react with water to generate OH•, which helps in the oxidation of CIP and its consequent degradation. Simultaneously, the reaction of h⁺ with water also leads to the formation of OH•. For the FeOOH/C composite, the photogenerated holes located in VB have E_(h⁺) of +2.92 eV, which is more positive than E_(OH•/H₂O) (+2.68 eV) and, hence, it reacts with water to form OH•. However, the formation of O₂^{-•} is hindered since E_(e⁻) is +0.53 eV, which is lower than E_(O₂/O₂^{-•}) (+0.13 V). Consequently, there is no production of OH• through the photogenerated electrons. As is evident from the radical scavenging studies, it is clearly seen that h⁺ play a major role in the photocatalytic degradation of CIP. The scavenging of OH• radicals also affects the rate of photodegradation, but it is not as severe as that of h⁺. E_(h⁺) has a high positive potential, which signifies a high oxidizing power, which can act directly on the CIP adsorbed on the photocatalyst surface. Similar observations have been made in the case of CIP photodegradation over CeO₂/ZnO nanocomposites in the presence of UV light [9].

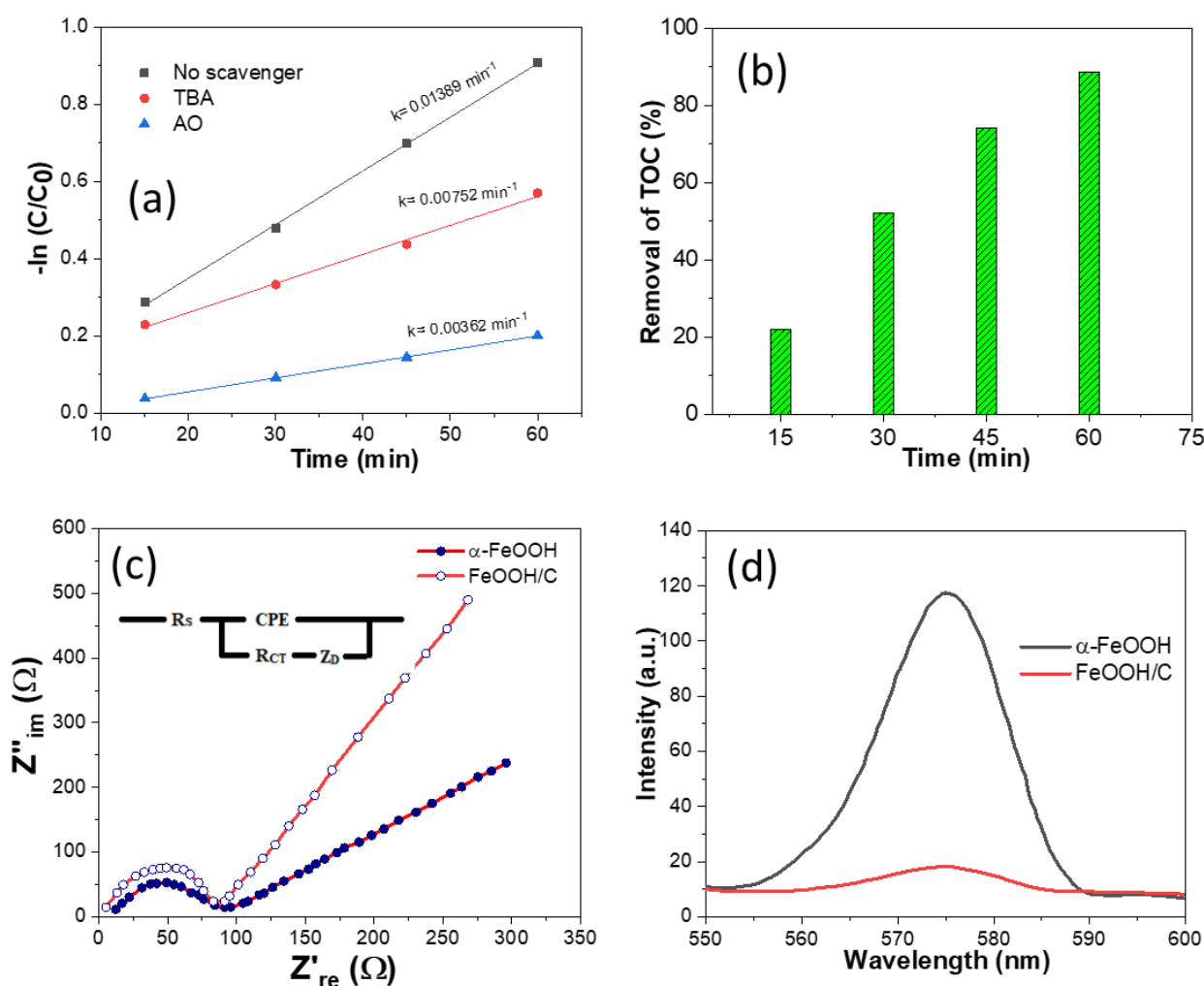


Figure 5. (a) Kinetics plot of the FeOOH/C composite in the presence of scavengers, (b) removal of total organic content with time using the FeOOH/C composite, (c) EIS spectrum and (d) PL spectrum of α -FeOOH and the FeOOH/C composite.

To check whether CIP has photodegraded to smaller organic molecules or has mineralized completely in the presence of the FeOOH/C composite, the total organic carbon content in the initial reaction mixture and that remaining after every 15 min of photo irradiation was monitored and the results are shown in Figure 5b. The carbon content in the mixture was $\sim 11.3\%$ after 60 min of photoirradiation, which indicates substantial mineralization of CIP.

There is an increase in the photodegradation efficiency when using the FeOOH/C composite compared to α -FeOOH. The addition of carbon generally leads to more efficient charge separation, which enhances the photodegradation process. To confirm this, EIS spectra of α -FeOOH and the FeOOH/C composite were recorded, and the corresponding Nyquist plot is shown in Figure 5c. The plot depicts a semi-circle in the high frequency region and a sloped straight line at low frequency. The former is related to the charge transfer impedance in the material and the latter corresponds to the ion-diffusion process in the solid phase. It is evident that in case of α -FeOOH, the diameter of the semi-circle is slightly larger than in case of the FeOOH/C composite, indicating lower charge transfer resistance in the latter. The data has been fitted with an appropriate equivalent circuit by using Z-view software (inset of Figure 5c). R_s refers to the bulk resistance, which arises from the combination of sheet and contact resistance in the system [25–27]. The R_s and charge transfer resistance (R_{ct}) value decreases in the FeOOH/C composite compared to α -FeOOH, signifying a decrease in the resistance and better conductivity, which is

normally expected in carbon composites. The R_{ct} of the FeOOH/C composite is $\sim 79.4 \Omega$, which is lower than that of α -FeOOH ($\sim 84.0 \Omega$). This signifies faster transportation of the photogenerated electron and holes in the FeOOH/C composite, which improves the photodegradation efficiency.

This is further verified by the photoluminescence (PL) spectrum of α -FeOOH and the FeOOH/C composite, which is a well-known technique to estimate the efficiency of the separation of photogenerated charge carriers. Low PL intensity signifies that the rate of recombination of the photogenerated e^-/h^+ is slow, which indicates that their separation is efficient. The PL spectra of α -FeOOH and the FeOOH/C composite are shown in Figure 5d, and it is evident that the PL intensity in the case of the latter is much less compared to the former. The results corroborate with those obtained from the EIS studies, which indicates that the improvement in the photocatalytic efficiency in the case of the FeOOH/C composite is due to the enhancement of the photoinduced charge separation. Apart from this, the presence of carbon in α -FeOOH increased the extent of visible light absorption, as is evident from the UV-vis absorption spectra, which is also advantageous for photocatalytic degradation. Carbon also acts as a dispersing medium for α -FeOOH and the increased surface area leads to the availability of a greater number of photoreactive sites in the material.

For practical application of a photocatalyst, its reusability and stability are critical factors. The reusability of the FeOOH/C composite has been tested for five consecutive cycles of CIP photodegradation. The activity reduced to $\sim 79\%$ CIP photodegradation after five cycles (Figure 6a), which is slightly less than that obtained in the first run (87%). The powder XRD of the FeOOH/C composite after five cycle runs is shown in Figure 6b and there are no obvious impurity peaks, which confirms the stability of the FeOOH/C composite.

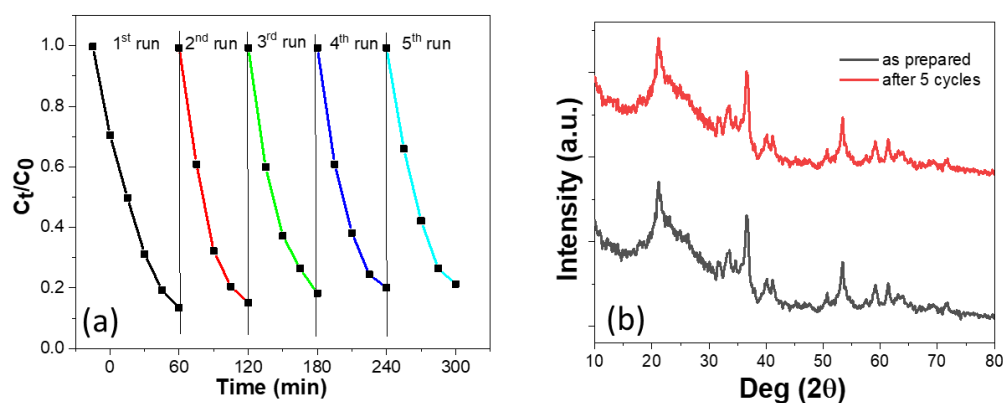


Figure 6. (a) Reusability study for 5 cycles of the FeOOH/C composite and (b) the pre- and post-run XRD of the FeOOH/C composite.

3. Materials and Methods

3.1. Materials

The AR grade ferrous sulphate heptahydrate ($\text{FeSO}_4 \cdot 7\text{H}_2\text{O}$), sodium hydroxide (NaOH) and ciprofloxacin ($\text{C}_{17}\text{H}_{18}\text{FN}_3\text{O}_3$) used in this work was purchased from Sigma Aldrich, Bengaluru, India. The Indian blackberry seeds were purchased from local fruit vendors in Mumbai, India.

3.2. Synthesis of Adsorbents

3.2.1. Synthesis of α -FeOOH

$\text{FeSO}_4 \cdot 7\text{H}_2\text{O}$ (8.52 g, 30.65 mmol) was dissolved in water and then NaOH was added to it until the pH of the solution changed to 9. The solution was sonicated under ambient atmosphere for 60 min with a power of 100 W/cm^2 at a frequency of 40 kHz using an ultrasonicator (Oscar Ultrasonics). The ochre precipitate obtained was centrifuged out and

washed with deionized water repeatedly. The product was heated in a furnace at 130 °C for 2 h.

3.2.2. Synthesis of Carbon

The Indian blackberry seeds were washed thoroughly with water several times and then dried under the sun. After attaining constant weight, they were ground in a mixer, transferred to an alumina boat and heated in a furnace under an oxygen-starved condition at 500 °C for 2 h. The residue was washed repeatedly with deionized water and dried in an ambient atmosphere.

3.2.3. Synthesis of α -FeOOH/carbon composite

A NaOH solution (0.01 M) was added dropwise to an aqueous solution of FeSO₄·7H₂O (5 g, 17.98 mmol) and the pH was adjusted to ~9. The solution was sonicated for 60 min using an ultrasonicator (100 W/cm², 40 kHz) under ambient pressure and temperature. Carbon (1 g) obtained from Indian blackberry seeds was added to it and sonicated for 10 min. The precipitate was centrifuged and washed repeatedly with distilled water and then heated in a furnace under an oxygen-starved condition at 130 °C for 2 h.

3.3. Characterization

The powder XRD of the samples were recorded on a PANalytical X-Pert Pro instrument (Almelo, Netherlands) using CuK α ($k = 1.5406$ and 1.5444\AA) radiation. The SEM images were recorded on a Hitachi SU-1510 (Tokyo, Japan). The morphology of the samples was checked by TEM using a Libra Zeiss 120 KeV (Jena, Germany) instrument. The samples were sonicated in ethanol and then placed on the carbon-coated copper grids for recording TEM images. The specific surface area was analysed using the Brunauer–Emmett–Teller (BET) method (Bel Japan Inc., Japan, Belsorp II) via nitrogen adsorption. Before starting the experiment, the samples were degassed at 100 °C for 8 h under argon flow. The UV-visible spectra of the pollutants were recorded using a Shimadzu UV-1650PC UV-visible spectrophotometer (Kyoto, Japan). For the zeta-potential measurements, a ZetaProbe analyser (Colloid Dynamics, Ponte Vedra Beach, FL, USA) was used.

3.4. Photocatalytic Studies

All photocatalytic experiments were repeated at least two times and the average values have been reported. The pH adjustments were performed by adding 0.05 M HCl or 0.05 M NaOH.

Ciprofloxacin Photodegradation

A total of 100 mg L⁻¹ of ciprofloxacin (CIP) stock solution was prepared by 45 min ultrasonication of aqueous dispersion of CIP powder in deionised water. This stock solution was diluted to predetermined concentrations for further experiments. In a typical procedure, 2.5 mg of the photocatalyst was added to 100 mL of the CIP solution (10 mg L⁻¹) and lightly stirred. The irradiation was performed using a 150 W Xe lamp. After every 15 min time interval, 3 mL of the solution was syringed out using a 0.20 μ m microfilter fitted syringe, poured in a quartz cuvette and the CIP concentration in the filtrate was analysed spectrophotometrically by checking the absorption at λ_{max} of 273 nm. The solution in the cuvette was added back to the main solution to maintain a constant volume during the course of the entire experiment. The effect of the concentration of photocatalyst on the adsorption process was investigated.

The removal efficiency (E_{eff}) of the photocatalyst for ciprofloxacin was calculated using the following equation:

$$E_{\text{eff}} = \frac{(C_0 - C_e)}{C_0} \times 100\% \quad (4)$$

where C_0 denotes the initial concentration of the pollutant analysed, C_e represents the equilibrium residual pollutant concentration remaining after the adsorption process, V denotes the volume of the solution (in mL) and m is the mass of the adsorbent used (in g).

Scavengers like 2-propanol and EDTA- Na_2 in 10 ppm concentration were added into the mixture during the photocatalytic degradation to assess the role played by HO^\bullet and h^+ , respectively, in the process. The total concentration of organic carbon in the mixtures was deduced using a TOC-L Shimadzu (Kyoto, Japan) instrument.

4. Conclusions

From this study, it has been established that the CIP photodegradation efficiency is enhanced when it forms a nanocomposite with carbon derived from the seeds of Indian blackberry. The waste material, which acts as an inexpensive source of carbon, could also be processed using a simple technique. The carbon addition favored greater adsorption of CIP and its photodegradation rate was almost doubled in the case of the FeOOH/C composite compared to that obtained in the case of α -FeOOH under visible light irradiation. This enhanced photocatalytic efficiency of FeOOH/C has been attributed to the structural modifications which increased the surface area, enhanced the quantum of visible light absorption and also provided a pathway for efficient charge carrier separation. The dominant role played by the photogenerated h^+ in the degradation of CIP has been established through radical scavenger studies. The reduction in total carbon content after the photodegradation of CIP has been confirmed. The stability and reusability of the FeOOH/C composite makes it a good choice for its practical application as a photocatalyst for CIP degradation.

Author Contributions: Conceptualization, D.P.D.; formal analysis, D.P.D.; methodology, S.A.; investigation, S.A.; writing—original draft preparation, D.P.D.; writing—review and editing, D.P.D.; visualization, D.P.D.; supervision, D.P.D.; project administration, D.P.D. All authors have read and agreed to the published version of the manuscript.

Funding: This research received no external funding.

Data Availability Statement: The data presented in this article are sharable on request to the corresponding author.

Conflicts of Interest: The authors declare no conflict of interest.

References

1. de Ilurdoz, M.S.; Sadhwani, J.J.; Reboso, J.V. Antibiotic removal processes from water & wastewater for the protection of the aquatic environment-A review. *J. Water Process Eng.* **2022**, *45*, 102474.
2. Babic, S.; Perisa, M.; Skoric, I. Photolytic degradation of norfloxacin, enrofloxacin and ciprofloxacin in various aqueous media. *Chemosphere* **2013**, *91*, 1635–1642. [[CrossRef](#)]
3. Wang, J.; Zhuan, R. Degradation of antibiotics by advanced oxidation processes: An Overview. *Sci. Total Environ.* **2020**, *701*, 135023. [[CrossRef](#)]
4. Zhu, Z.; Zhou, Q. Action and mechanism of semiconductor photocatalysis on degradation of organic pollutants in water treatment: A review. *Environ. Nanotech. Monit. Manag.* **2019**, *12*, 100255. [[CrossRef](#)]
5. Liu, H.-Y.; Niu, C.-G.; Guo, H.; Huang, D.-W.; Liang, C.; Yang, Y.-Y.; Tang, N.; Zhang, X.-G. Integrating the Z-scheme heterojunction and hot electrons injection into a plasmonic-based $\text{Zn}_2\text{In}_2\text{S}_5/\text{W}_{18}\text{O}_{49}$ composite induced improved molecular oxygen activation for photocatalytic degradation and antibacterial performance. *J. Coll. Interface Sci.* **2022**, *610*, 953–969. [[CrossRef](#)] [[PubMed](#)]
6. Yang, Y.Y.; Niu, C.-G.; Huang, D.-W.; Guo, H.; Feng, H.-P.; Li, L.; Liu, H.-Y.; Fan, Q.-Q.; Qin, M.-Z. Appropriate oxygen vacancies and Mo-N bond synergistically modulate charge transfer dynamics of $\text{MoO}_{3-x}/\text{S-CN}$ for superior photocatalytic disinfection: Unveiling synergistic effects and disinfection mechanism. *J. Hazard. Mater.* **2023**, *445*, 130481. [[CrossRef](#)]
7. Yang, Y.-Y.; Feng, H.-P.; Niu, C.-G.; Huang, D.-W.; Guo, H.; Liang, C.; Liu, H.-Y.; Chen, S.; Tang, N.; Li, L. Constructing a plasma-based Schottky heterojunction for near-infrared-driven photothermal synergistic water disinfection: Synergetic effects and antibacterial mechanisms. *Chem. Eng. J.* **2021**, *426*, 131902. [[CrossRef](#)]
8. Medhi, R.; Marquez, M.D.; Lee, T.R. Visible-light-active doped metal oxide nanoparticles: Review of their synthesis, properties, and applications. *ACS Appl. Nano Mater.* **2020**, *3*, 6156–6185. [[CrossRef](#)]
9. Wolski, L.; Grzelak, K.; Muńko, M.; Frankowski, M.; Grzyb, T.; Nowaczyk, G. Insight into photocatalytic degradation of ciprofloxacin over CeO_2/ZnO nanocomposites: Unravelling the synergy between the metal oxides and analysis of reaction pathways. *Appl. Surface Sci.* **2021**, *563*, 150338. [[CrossRef](#)]

10. Wen, X.-J.; Niu, C.-G.; Zhang, L.; Liang, C.; Guo, H.; Zeng, G.-M. Photocatalytic degradation of ciprofloxacin by a novel Z-scheme CeO₂-Ag/AgBr photocatalyst: Influencing factors, possible degradation pathways, and mechanism insight. *J. Catal.* **2018**, *358*, 141–154. [[CrossRef](#)]
11. Zhou, X.; Yang, H.; Wang, C.; Mao, X.; Wang, Y.; Yang, Y.; Liu, G. Visible light induced photocatalytic degradation of rhodamine B on one-dimensional iron oxide particles. *J. Phys. Chem. C* **2010**, *114*, 17051–17061. [[CrossRef](#)]
12. Ruales-Lonfat, C.; Barona, J.F.; Sienkiewicz, A.; Bensimon, M.; V´elez-Colmenares, J.; Ben´itez, N.; Pulgar´ın, C. Iron oxides semiconductors are efficient for solar water disinfection: A comparison with photo-Fenton processes at neutral pH. *Appl. Catal. B* **2015**, *166–167*, 497–508. [[CrossRef](#)]
13. Pervez, M.N.; Ma, S.; Huang, S.; Naddeo, V.; Zhao, Y. Photo-Fenton Degradation of Ciprofloxacin by Novel Graphene Quantum Dots/ α -FeOOH Nanocomposites for the production of safe drinking water from surface water. *Water* **2022**, *14*, 2260. [[CrossRef](#)]
14. Dutta, D.P. Composites of Sb₂O₄ and biomass-derived mesoporous disordered carbon as versatile anodes for sodium-ion batteries. *ChemSelect* **2020**, *5*, 1846.
15. Araga, R.; Soni, S.; Sharma, C.S. Fluoride adsorption from aqueous solution using activated carbon obtained from KOH-treated jamun (*Syzygium cumini*) seed. *J. Environ. Chem. Eng.* **2017**, *5*, 5608–5616. [[CrossRef](#)]
16. Raj, K.A.; Panda, M.R.; Dutta, D.P.; Mitra, S. Bio-derived mesoporous disordered carbon: An excellent anode in sodium-ion battery and full-cell lab prototype. *Carbon* **2019**, *143*, 402–412. [[CrossRef](#)]
17. Abrashev, M.V.; Ivanov, V.G.; Stefanov, B.S.; Todorov, N.D.; Rosell, J.; Skumryev, V. Raman spectroscopy of alpha-FeOOH (goethite) near antiferromagnetic to paramagnetic phase transition. *J. Appl. Phys.* **2020**, *127*, 205108. [[CrossRef](#)]
18. Vernekar, D.; Jagadeesan, D. Tunable acid–base bifunctional catalytic activity of FeOOH in an orthogonal tandem reaction. *Catal. Sci. Technol.* **2015**, *5*, 4029. [[CrossRef](#)]
19. Sharma, S.; Kaur, M.; Sharma, C.; Choudhary, A.; Paul, S. Biomass-Derived Activated Carbon-Supported Copper Catalyst: An Efficient Heterogeneous Magnetic Catalyst for Base-Free Chan–Lam Coupling and Oxidations. *ACS Omega* **2021**, *6*, 19529–19545. [[CrossRef](#)]
20. Yamashita, T.; Hayes, P. Analysis of XPS spectra of Fe²⁺ and Fe³⁺ ions in oxide materials. *Appl. Surf. Sci.* **2008**, *254*, 2441–2449. [[CrossRef](#)]
21. Fang, D.; Yu, Y.; Xu, Z.; Liang, J.; Zhou, L. Enhanced catalytic performance of β -FeOOH by coupling with single-walled carbon nanotubes in a visible-light-Fenton-like process. *Sci. Eng. Comp. Mater.* **2018**, *25*, 9–15. [[CrossRef](#)]
22. Huang, H.W.; Li, X.W.; Wang, J.J.; Dong, F.; Chu, P.K.; Zhang, T.R.; Zhang, Y.H. Anionic group self-doping as a promising strategy: Band-gap engineering and multi-functional applications of high-performance CO₃²⁻-doped Bi₂O₂CO₃. *ACS Catal.* **2015**, *5*, 4094–4103. [[CrossRef](#)]
23. He, Z.Q.; Wang, D.; Fang, H.Y.; Chen, J.M.; Song, S. Highly efficient and stable Ag/AgIO₃ particles for photocatalytic reduction of CO₂ under visible light. *Nanoscale* **2014**, *6*, 10540. [[CrossRef](#)] [[PubMed](#)]
24. Dutta, D.P.; Ballal, A.; Chopade, S.; Kumar, A. A study on the effect of transition metal (Ti⁴⁺, Mn²⁺, Cu²⁺ and Zn²⁺)-doping on visible light photocatalytic activity of Bi₂MoO₆ nanorods. *J. Photochem. Photobiol. A Chem.* **2017**, *346*, 105–112. [[CrossRef](#)]
25. Zhang, T.; Lv, C.; Wang, X.; Wang, S.; Xie, Y.; Yu, M.; Sun, C.; Pan, K. Surface active-site engineering in NiCoSe₂/nitrogen-doped carbon dodecahedrons for efficient triiodide reduction in photovoltaics. *Appl. Surf. Sci.* **2023**, *610*, 155483. [[CrossRef](#)]
26. Song, T.; Zhang, Z.; Zhao, B.; Wang, L.; Kan, W.; Sun, L.; Wang, X. Boosting catalytic performance of hierarchical Co/Co_{0.85}Se microspheres via Mott-Schottky effect toward triiodide reduction and alkaline hydrogen evolution. *J. Alloys Compd.* **2022**, *918*, 165608. [[CrossRef](#)]
27. Liu, Z.; Xin, W.; Xie, W.; Wang, X.; Li, N.; Yuan, Z.; Li, Y.; Wang, J. Integration of hierarchical tin Sulfide@Sulfur-Doped carbon porous composites with enhanced performance for triiodide reduction. *Dyes Pigm.* **2022**, *204*, 110458. [[CrossRef](#)]

Disclaimer/Publisher’s Note: The statements, opinions and data contained in all publications are solely those of the individual author(s) and contributor(s) and not of MDPI and/or the editor(s). MDPI and/or the editor(s) disclaim responsibility for any injury to people or property resulting from any ideas, methods, instructions or products referred to in the content.